EurJIC
European Journal of Inorganic Chemistry

Research Article
doi.org/10.1002/ejic.202200684

Chemistry Europe
European Chemical Societies Publishing

www.eurjic.org

Synthesis of [FeFe] Hydrogenase Mimics with Lipoic acid and its Selenium Analogue as Anchor Groups

Stefan Benndorf,[a] Sihem Groni,[b] Leanne M. Stafast,[a] Helmar Görls,[a] Claire Fave,[b] Bernd Schöllhorn,*[b] and Wolfgang Weigand*[a, c]

[FeFe] hydrogenase (H_2ase) mimicking complexes containing lipoic and selenolipoic acid moieties connected to 2-hydroxy-1,3-dithiopropane and 2-hydroxy-1,3-diselenopropane bridging ligands were synthesized and characterized using different spectroscopic methods. X-ray diffraction analysis was utilized to determine the molecular structure of a triphenylphosphane substituted analogue. Cyclic voltammetry (CV) investigations on the redox chemistry in presence and absence of acetic acid (AcOH) revealed differing behaviours among the mimics. IR spectroelectrochemistry (IR SEC) enabled deeper insights of structural changes during electrochemical measurements. The elaboration of surface confined systems was studied in preliminary experiments. CV experiments showed that the lipoic acid derivatives of the [FeFe] H_2ase mimics formed well-organized self-assembled monolayers (SAMs) on Pt electrodes, a promising result for future work.

Introduction

Numerous mimics of the active site of natural [FeFe] H_2ase enzymes were synthesized and analysed during the last decades, frequently accompanied by demonstrations of their catalytic activity regarding dihydrogen formation in electro and photochemical experiments.[1,2]

One significant issue in electrolysis and photocatalysis is the diffusion-limited transport of the catalytic centre to the electrode, that is necessary for an effective electron transfer.[3,4] Immobilizing [FeFe] H_2ase enzymes or model complexes on the electrode surface to attain chemically modified electrodes were realized by electrostatic adsorption,[5] embedding in redox-active hydrogels or polymers,[6] absorption into mesoporous electrodes,[7] reduction of diazonium salt spacers on carbon electrodes,[8,9] by carboxylic acid group on fluorine-doped tin oxide (FTO) or nickel oxide electrodes,[10,11] and thiol spacer groups on gold electrodes, with a functional moieties for further modification with the [FeFe] H_2ase mimic or enzyme, amongst others.[4,12] However, [FeFe] H_2ase mimics attached to electrodes lack consistency and high activity during the catalytic process, due to their sensitivity regarding high pH values or oxygen and irreversible electrocatalytic behaviour.[8,13] Additionally, *Reek* et al. surmised the depletion of the substrates was caused by hydrolysis of the carboxylate anchor groups from the FTO surface.[10]

Our approach is to use dithiolane or diselenolane anchoring groups with a great affinity to gold and platinum and the capability to form stable SAMs under electrochemical conditions.[3,14,15] Due to their adjustable reactivity, disulfide moieties gained great interest in the fields of biochemistry, organic synthesis, catalysis and coordination chemistry, amongst others.[16] Furthermore, they show versatile electrochemical behaviour, including the formation of a variety of lipoic acid S-oxides, the reduction to radical species, dimers and higher polymers to the point of dihydrolipoic acid.[17]

Lipoic and selenolipoic acid were connected to 2-hydroxy-1,3-propandithiolate (pdt-2-OH)[18] or 2-hydroxypropandiselenolate (pds-2-OH)[19] [FeFe] H_2ase mimics via esterification,[20] giving four complexes with the possible permutations distributing S and Se at the iron cluster along with the anchor group. They were analysed in terms of X-ray diffraction analysis, CV in the presence and absence of AcOH and IR SEC. In first experiments the H_2ase mimics were immobilized as self-assembled monolayers on Au and Pt electrodes. The electrochemical properties and the stability of the formed SAMs was investigated by CV in order to evaluate their potential as surface confined electrocatalytical systems.

[a] *S. Benndorf, L. M. Stafast, Dr. H. Görls, Prof. Dr. W. Weigand*
Institute of Inorganic and Analytical Chemistry
Friedrich Schiller University Jena
Humboldtstrasse 8, 07743 Jena (Germany)
E-mail: wolfgang.weigand@uni-jena.de
https://www.chemgeo.uni-jena.de/weigand
[b] *Dr. S. Groni, Dr. C. Fave, Prof. Dr. B. Schöllhorn*
Université Paris Cité
Laboratoire d'Electrochimie Moléculaire
F-75013 Paris (France)
E-mail: claire.fave@u-paris.fr
bernd.schollhorn@u-paris.fr
http://www.lemp7.cnrs.fr/directories/personal/B_Schollhorn_en.htm
[c] *Prof. Dr. W. Weigand*
Center for Energy and Environmental Chemistry Jena (CEEC Jena)
Jena Center of Soft Matter
Friedrich Schiller University Jena
Philosophenweg 7a, 07743 Jena (Germany)

Supporting information for this article is available on the WWW under https://doi.org/10.1002/ejic.202200684

Research Article
doi.org/10.1002/ejic.202200684

Results and Discussion

Synthesis of [FeFe] H_2ase model complexes 2, 3, 5, 6 and 7

The synthesis of complex **1** was carried out by use of a novel synthetic pathway developed recently in our group, to generate [FeFe] H_2ase model complexes more efficiently, by using *N*-methyl-2-pyrrolidone (NMP) as an additive. The precursor 1,3-disulfanylpropane-2-ol was dissolved in NMP and toluene at 50 °C. Triirondodecacarbonyl ($Fe_3(CO)_{12}$) was added in one portion and the resulting solution was stirred for ten minutes, until the dark green solution became dark red, affording target complex **1** as a red solid after purification (Scheme 1).[21]

Complex **4** was synthesized by refluxing freshly prepared 1,3-bis(selenocyanato)propane-2-ol[22] and $Fe_3(CO)_{12}$ in THF for 1 h, adapted from *Harb* et al.,[23,24] and obtained as a red solid after purification (Scheme 1).

The syntheses of complexes **2**, **3**, **5** and **6** were carried out by a modified Steglich esterification procedure of [FeFe] H_2ase mimics **1** or **4** with lipoic acid or selenolipoic acid, respectively, in the presence of *N*,*N*′-dicyclohexylcarbodiimide (DCC) and 4-dimethylaminopyridine (DMAP).[20] The resulting compounds were isolated as red, high-viscous oils (Scheme 1). To analyze the influence of triphenylphosphane (PPh_3) as a better σ donor concerning electrochemical behaviour, one CO-ligand was replaced by synthesis of complex **7**. By mixing compound **2** and trimethylamine *N*-oxide dihydrate in dichloromethane (DCM) for 20 min, adding one equivalent of PPh_3 and stirring for 15 h at room temperature (RT), target complex **7** was isolated as a brown solid (Scheme 2).[21]

Molecular structure

Exemplarily, Figure 1 shows one of the three conformers (Figure S1) of the molecular structure of compound **7**. The structure revealed the characteristic butterfly conformation of the [Fe_2S_2] cluster. The coordination sphere in the vicinity of each Fe atom can be described as a distorted octahedron with two S atoms, each linked to both Fe centres, and three terminal CO ligands for Fe1 and two terminal CO ligands and a PPh_3 ligand for Fe2. Due to the electron density donating properties of PPh_3 the Fe–Fe (2.5265(8) Å) bond length is elongated in comparison to the Fe–Fe (2.5039(6) Å) bond length of compound **1**, published by our group,[18] however, in good agreement with the PPh_3 substituted derivative of complex **1**, Fe–Fe (2.5255(8) Å), synthesized by *Song* and co-workers.[26] Furthermore, the lipoic acid moiety is arranged around the apical located PPh_3 ligand, indicating minor attractive interactions.

Electrochemical Investigation

To study the influence of sulfur and selenium as well as the substituting of one CO ligand in complex **2** by PPh_3 toward electrochemical behaviour, CV was carried out on complexes **2**, **3**, **5**, **6** and **7** in 0.1 M [*n*-Bu_4N][BF_4] acetonitrile (MeCN) solutions,

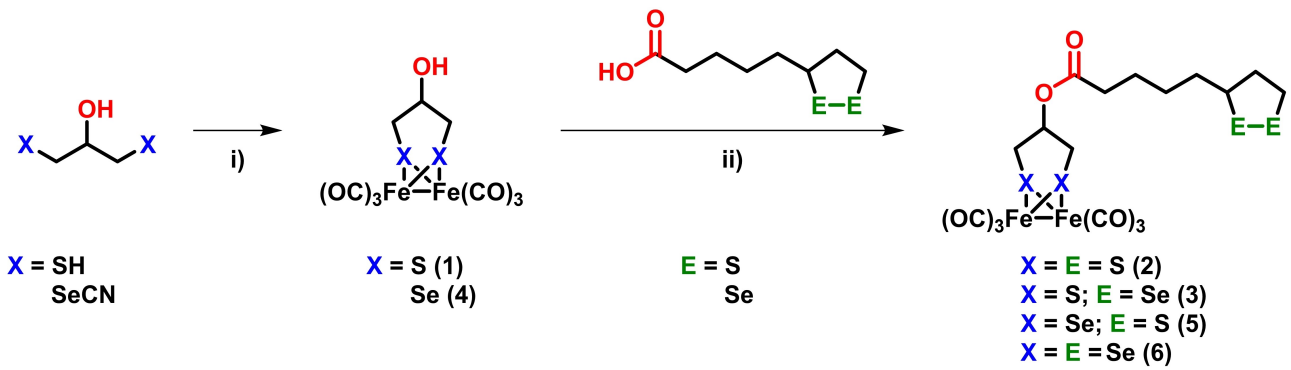

Scheme 1. Synthesis route for [FeFe] H_2ase mimics **1**–**6**; i) $Fe_3(CO)_{12}$, toluene, NMP, 50 °C, 10 min;[21] (**1**) $Fe_3(CO)_{12}$, THF, reflux, 1 h (**4**)[23]; ii) DCC, DMAP, DCM, RT, 14 h.[20]

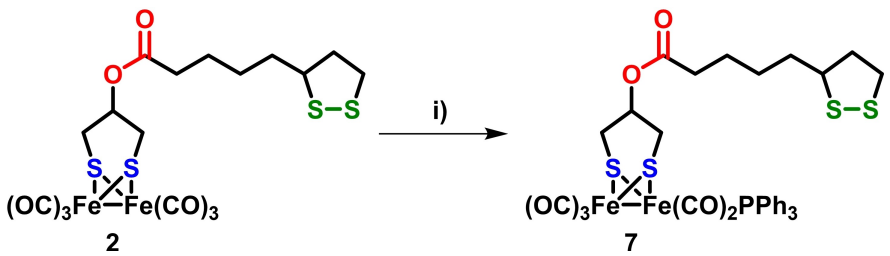

Scheme 2. Synthesis route for [FeFe] H_2ase mimics **7**; i) trimethylamine *N*-oxide dihydrate, PPh_3, DCM, RT, 15 h.[25]

Research Article
doi.org/10.1002/ejic.202200684

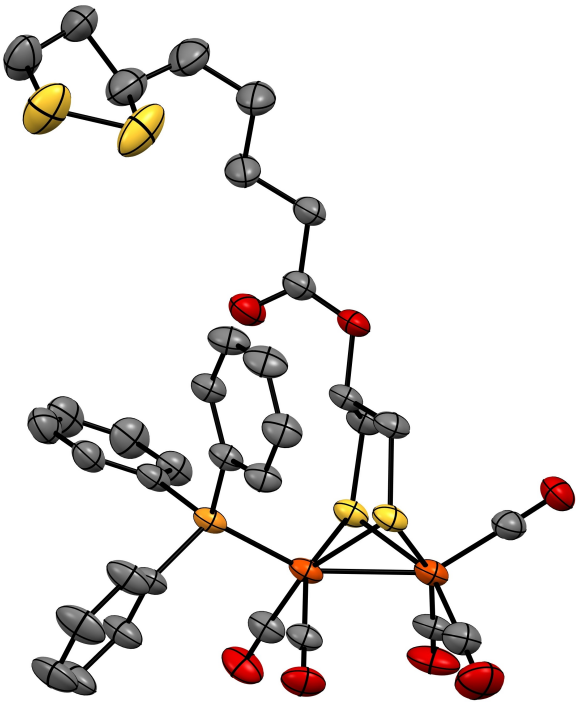

Figure 1. Molecular structure of complex **7**. The ellipsoids represent a probability of 50 %, (hydrogen atoms were omitted for clarity). Legend of the colour code: C (grey), O (red), S (yellow), Fe (orange), P (salmon).

as depicted in Figure 2 and S6. The CV of compound **2** (Figure 2, grey) reveals one partially reversible reduction at $E_{pc}^{1} = -1.57$ V, assigned to the one-electron-reduction of [$Fe^{I}Fe^{I}$] to [$Fe^{0}Fe^{I}$] with a linear scan rate dependence of the current function (Figure S2), and two non-reversible reduction events at $E_{pc}^{2} = -1.75$ V and $E_{pc}^{3} = -2.28$ V (Figure 2). At higher scan rates, E_{pc}^{2} fades, and the reversibility of the first reduction process is enhanced (Figure S3), indicated by a rise of the anodic-to-

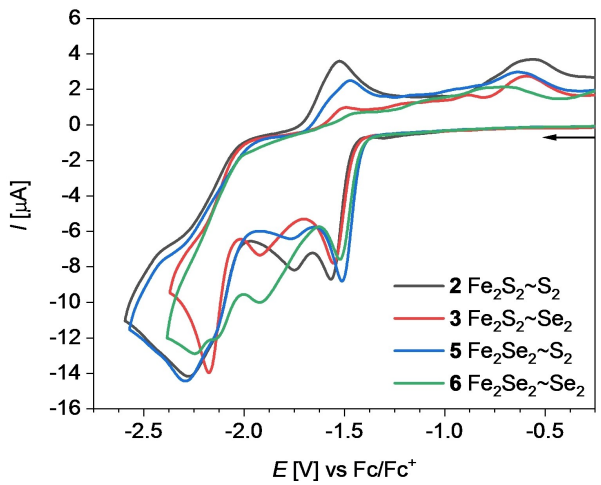

Figure 2. Cyclic voltammograms ($\nu = 0.2$ V/s) of compounds **2**, **3**, **5** and **6** ($c = 1$ mmol/L) in N_2-purged MeCN/[*n*-Bu_4N][BF_4] (0.1 mol/L) at RT. The arrow indicates the scan direction. The potential *E* is given in V and referenced to the Fc/Fc^+ couple.

cathodic peak current ratio (I_{pa}/I_{pc}). This behaviour implies an irreversible follow-up reaction appearing after the first reduction as described before.[27] The electrochemical analysis of compound **5** (blue) shows a similar behaviour for its reduction events. Both complexes are linked to lipoic acid, which might cause a follow-up reaction, forming side products, however, the reduction of lipoic acid occurs at more negative potentials (Figure S5).[14] The third reduction process at $E_{pc}^{4} = -2.28$ V and its shoulder signal at $E_{pc}^{3} = -2.13$ V are assigned to the second electron uptake of the iron center and the reduction of the sulfur-sulfur bond of the lipoic acid moiety, interfering with each other.[14,18,19,28] As a result, these overlapping reduction events show a broadened peak. Nevertheless, it should be noted, that the reduction of the dithiolane bridge is shifted by $\Delta E_{pc}^{S-S} = 150$ mV at least to more positive values, compared to the pure lipoic acid (Figure S5). This occurrence might include an irreversible interaction between dithiolane sulfur atoms and the iron centre, which facilitates the electron uptake.

On the contrary, complexes **3** (red) and **6** (green) are showing their second reduction event at $E_{pc}^{2} = -1.92$ V, which can be assigned to the reduction of the diselenolane bridge, by comparison with the pure precursor selenolipoic acid (Figure S6). This reduction process remains at higher scan rates and the reversibility of the first reduction rises among with the other reduction waves (Figure S4). The second reduction of the iron centres is assigned to the third event at $E_{pc}^{3} = -2.18$ V, in good agreement with their precursor complexes **1** and **4**, respectively.[18,19]

The potentials for the first reduction ([$Fe^{I}Fe^{I}$]→[$Fe^{0}Fe^{I}$]) differ from $\Delta E_{pc}^{1} = 30$–60 mV, among the sulfur and selenium containing iron centres, implying an influence on the electrochemical properties of the [FeFe] H_2ase mimicking complexes, due to the weaker electron-donating properties of the Se-containing ligands (Figure 3; Table 1). This behaviour is also observed for other S- and Se-containing [FeFe] H_2ase models.[23,27,29,30]

The substitution of one terminal carbonyl ligand at the iron core with electron-donating ligands, like PPh_3, induces a different electrochemical behaviour, caused by increased electron density at the iron center. The potential for the first reduction of compound **7** appears at $E_{pc}^{1} = -1.75$ V, exhibiting a shift to more negative potential by $\Delta E_{pc}^{1} = 180$ mV, compared to the first reduction event of **2** (Table 1), likewise to previously reported phosphane mono-substituted [FeFe] H_2ase mimics.[25,31,32] Additionally, the second non-reversible reduction, as described for compound **2**, vanishes or might be overlapped by the first electron uptake. However, the second occurring

Table 1. Summary of the reduction potentials of complexes **2**, **3**, **5**, **6** and **7**. Potentials *E* are given in V, referenced to the Fc/Fc^+ couple.

complex	E_{pc}^{1} [V]	E_{pc}^{2} [V]	E_{pc}^{3} [V]	E_{pc}^{4} [V]
2	−1.57	−1.75	−2.13[a]	−2.28
3	−1.55	−1.92	−2.18	
5	−1.51	−1.77	−2.13[a]	−2.29
6	−1.52	−1.92	−2.13	−2.25
7	−1.75	−2.13[a]	−2.30	

[a] This reduction event is appears as a weak shoulder.

Research Article
doi.org/10.1002/ejic.202200684

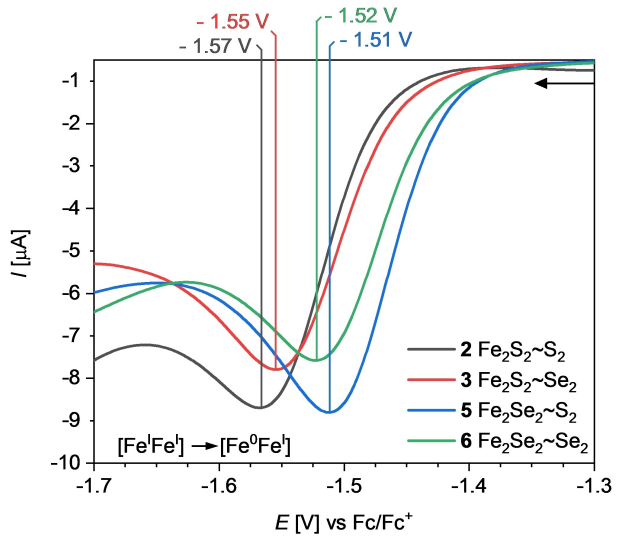

Figure 3. Cyclic voltammograms ($\nu = 0.2$ V/s) of the first reduction of compounds **2**, **3**, **5** and **6** ($c = 1$ mmol/L) in N_2-purged MeCN/[n-Bu_4N][BF_4] (0.1 mol/L) at RT. The arrow indicates the scan direction. The potential E is given in V and referenced to the Fc/Fc^+ couple.

reduction event of compound **7** indicates no remarkable shift for the assigned second reduction of the iron centre (Figure S7).[32]

To support these assignments, we took a closer look where the reduction events take place and how many electrons were involved, therefore, IR SEC investigations were performed, due to the high sensitivity of the $\tilde{\nu}$(CO) bands of metal carbonyls to the charge state and geometry of the complex.[33–35]

IR SEC investigations

IR SEC was carried out in an OTTLE (optically transparent thin layer electrochemical) cell (c(complex) = 2 mmol/L, MeCN, c(n-Bu_4NBF_4) = 0.1 mol/L).[36] The potential was raised in negative direction at slow scan rates ($\nu = 2$ mV/s, Figure S8) to study structural changes of the complexes during the electron uptake. Due to the use of different working (WE) and reference electrodes, the absolute potentials were shifted to less negative potentials, compared to prior electrochemical experiments.

Figures 4A and 4C show the spectroscopic changes for the first reduction step of compound **2**, between $E = -1.022$ V and $E = -1.190$ V. The observable bathochromic shift by $\Delta\,\tilde{\nu}$(CO) = 55–103 cm^{-1} of the terminal carbonyl signals (2078, 2039, 2000 cm^{-1}→2023, 1957, 1897 cm^{-1}), respectively, is caused by

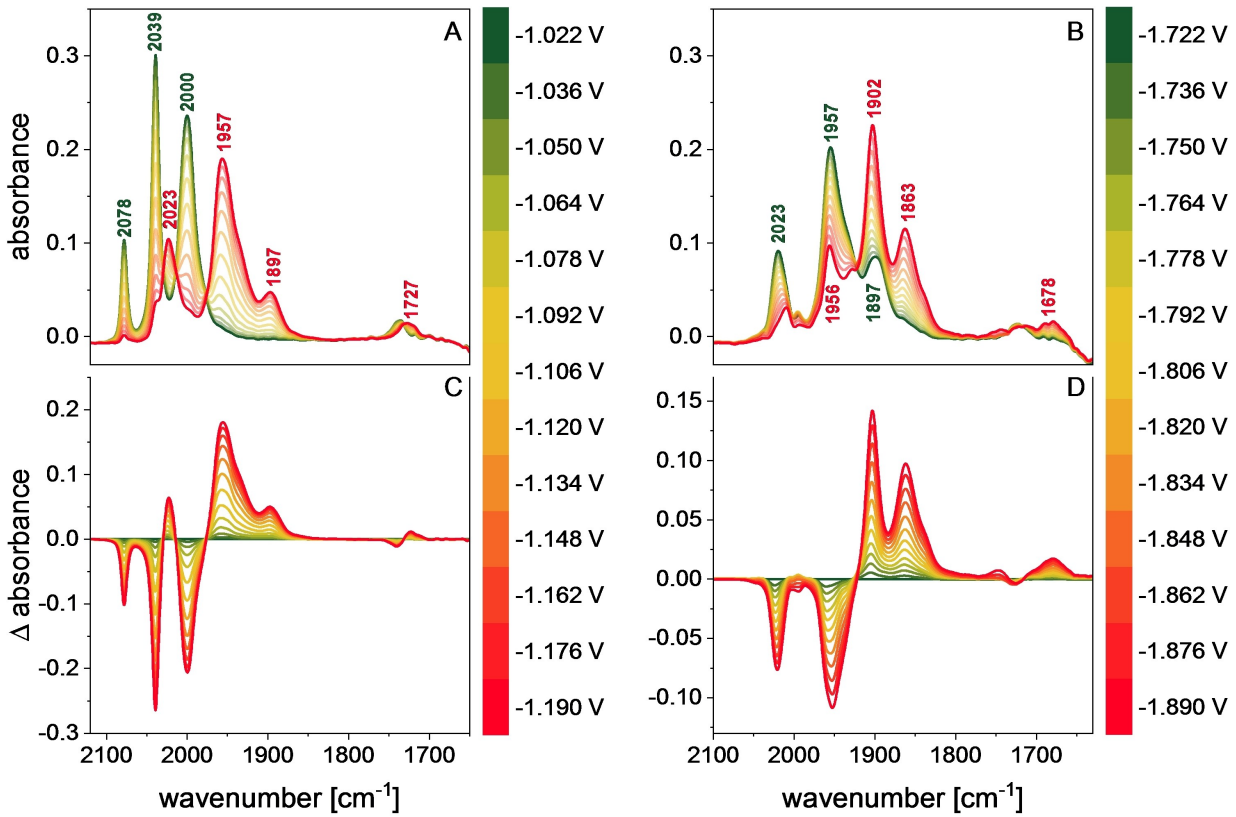

Figure 4. IR SEC measurements of the first (A) and second reduction (B) and their respective differential spectra (C, D) of compound **2** (MeCN, $c = 2$ mmol/L). The Δ absorbance spectra were calculated by subtracting a spectrum recorded immediately before the reducing phase. Keep in mind that there is a difference in cathodic shifts between the CV (glassy carbon WE, non-aqueous Ag/AgCl RE) and the IR SEC (Pt WE, Ag wire RE) experiments due to the use of different electrodes (for further details see SI).

Research Article
doi.org/10.1002/ejic.202200684

the increased electron density at the iron cores and the subsequent enhanced back donation to the anti-bonding π* orbital of the carbonyl ligands.[33,34,37] This change in the spectra is in good agreement with a one-electron reduction of [$Fe^{I}Fe^{I}$]→[$Fe^{0}Fe^{I}$], furthermore, the shape and ratio of the absorption bands is altering, indicating structural rearrangements after the electron uptake.[21,33,38,39,40] Additionally a new weak band occurs at $\tilde{\nu}(\mu\text{-CO}) = 1727\ cm^{-1}$, suggesting the formation of a bridging carbonyl.[33,41] However the CV of the SEC experiment show no peak between the first and second reduction of the iron centre (Figure S8), indicating that the second event E_{pc}^{2} is happening at the same time as the first reduction, due to the slow scan rate. The same experiment was performed with the precursor **1**, indicating differences in the spectroelectrochemical behaviour (see Figure S9). The spectra of complex **1** exhibit a pattern likewise to its $Fe_2(pdt)(CO)_6^-$ (pdt = propanedithiolate) analogue, defined by the formation of four partially separated absorption bands of the terminal carbonyl ligands and one bridging carbonyl $\tilde{\nu}(\mu\text{-CO}) = 1720\ cm^{-1}$.[21,33] The substitution with lipoic acid leads to differing behaviour during the electrochemical treatment of the complexes.

The spectroscopic changes during the second reduction of complex **2** between $E = -1.722$ V and $E = -1.890$ V are depicted in Figure 4B and its respective differential spectra (Figure 4D). The terminal carbonyl signals were shifted by $\Delta\tilde{\nu}(CO) = 33–66\ cm^{-1}$ (2023, 1957, 1897 cm^{-1}→1956, 1902, 1863 cm^{-1}), respectively. These values are indicating another one-electron reduction step, assigned to the reduction of [$Fe^{0}Fe^{I}$]→[$Fe^{0}Fe^{0}$]. The band of the bridging carbonyl is also bathochromically shifted to $\tilde{\nu}(\mu\text{-CO}) = 1678\ cm^{-1}$, and reveals a absorption pattern, likewise to the $Fe_2(bdt)(CO)_6^{2-}$ (bdt = benzenedithiolate) analogue, indicating structural rearrangements.[37,40]

Further reduction of compound **2** led to new absorption bands in the spectra (see Figure S10), subsequently evolving from product $\mathbf{2}^{2-}$, due to the increased charge and additional structural changes. A well-defined absorption band appeared at $\tilde{\nu} = 1745\ cm^{-1}$, that could be ascribed to the formation of tetracarbonyl ferrate, $[Fe(CO)_4]^{2-}$, which is assigned to be a degradation product during the excessive reduction of iron carbonyl complexes.[21,38,42,43] This appearance is consistent with the irreversible electrochemical behaviour (see Figure 2). At even more negative potential $E > -2.128$ V, another explicit band evolves at $\tilde{\nu} = 2118\ cm^{-1}$, which might be assigned to the formation of an (iso)thiocyanate species arising at the edge of the potential window of MeCN and its reaction with the reduced dithiolane bridge (Figure S10). Unfortunately, no sample of this product could be isolated for further investigations.

During the SEC experiments complexes **3**, **5** and **6** show similar behaviour as compound **2** (see Figure S11, S12 and S13, respectively). The reduction of the diselenolane bridge of complexes **5** and **6** caused only minor changes in the spectra (Figure S14), even though they were observable in the respective CV during the SEC (Figure S15).

The IR SEC of compound **7** exhibits an interesting performance (Figure S16). The resulting IR spectrum after the first reduction to $\mathbf{7}^{-}$ is almost identical to that of compound **2** in the mono-reduced state (Figure S17). The follow-up reduction of both compounds leads to almost very similar spectra as well, implying comparable complex geometry and electron density at the iron cores. These findings explain the same reduction potential (−2.13 V) and shape of the CV spectra for the second reduction event (Figure S7). Speculatively, one could assume that PPh_3 dissociates from **7** after the first reduction step and that the same species is formed when **2** is reduced to $\mathbf{2}^{-}$.

Electrocatalysis

To examine the catalytic features of complexes **2**, **3**, **5** and **6** regarding hydrogen production, CV in the presence of various amounts of AcOH in 0.1 M [*n*-Bu_4N][BF_4] MeCN solutions was performed. The behaviour of complex **2** is illustrated in Figure 5, defined by three reduction events at $E_{pc}^{1} = -1.56$ V, $E_{p}^{cat2} = -1.84$ V and $E_{p}^{cat3} = -2.17$ V. The addition of one equivalent of AcOH shifts the first reduction potential to more negative values by $\Delta E_{pc}^{1} = 50$ mV, compared to the pure complex. Additionally, the current is increased to the doubled value, indicating an additional electron uptake (Figure S18). Further addition of AcOH induces a potential shift to less negative potentials and the current increases, however, it levels off at four equivalents. This shift indicates a proton uptake, that is facilitated by raising amounts of AcOH. That supports the assumption that there is the uptake of two electrons while the mono-reduced species is usually not basic enough to be protonated by a weak acid such as AcOH.[44,45]

Another reduction appears at $E_{p}^{cat2} = -1.84$ V, that shows catalytic increase of the current, implying subsequent protonation and the potential dihydrogen-release to close a catalytic cycle. Additional electron uptake at $E_{p}^{cat3} = -2.16$ V enables the formation of another catalytic active species, that is capable to

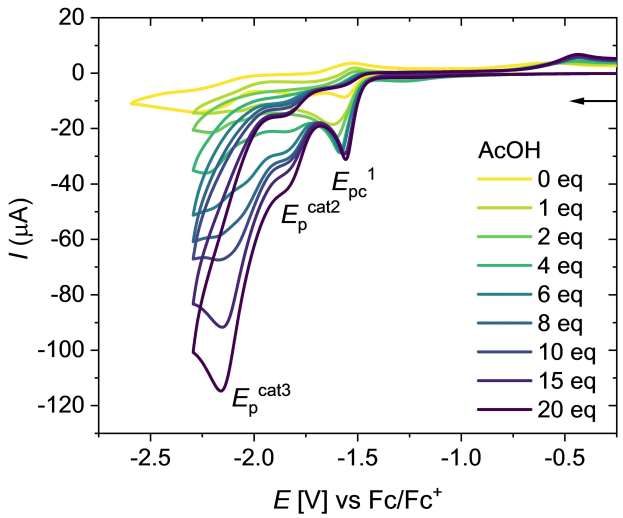

Figure 5. Cyclic voltammograms ($\nu = 0.2$ V/s) of compound **2** ($c = 1$ mmol/L) with various amounts of AcOH in N_2-purged MeCN/[*n*-Bu_4N][BF_4] (0.1 mol/L) at RT. The arrow indicates the scan direction. The potential *E* is given in V and referenced to the Fc/Fc^+ couple.

discharge dihydrogen. Scheme S1 demonstrates a potential catalytic cycle for the two processes at E_p^{cat2} and E_p^{cat3}.

This catalytic behaviour is similar to previously reported hexacarbonyl [FeFe] H_2ase mimics in the literature, that show a two electron reduction during the first reduction step.[27,30,42,44,46] Further increase of the reduction potential leads to another reduction event at $E_p^4 = -2.50$ V, that is attributed to the reduction of AcOH (Figure S19). The comparison to the same experiment utilizing complex **1** exhibits a similar behaviour, except the first reduction event, that does not show such a strong increase of the current (Figure S20 and S21). This observation supports the notion, that there is an influence of the lipoic acid moiety on the catalytic cycle.

The CV experiment of complex **3** shows a slightly different performance, indicated by two reduction events (Figure S22). The addition of AcOH shifts the first reduction event at $E_{pc}^1 = -1.55$ V to slightly more negative values by $\Delta E_{pc}^1 = 20$ mV, however, the current and the potential of this process remains constant after the addition of four equivalents. The second reduction event occurs at $E_p^{cat2} = -2.07$ V, showing no additional process at less negative potential, in comparison to complex **2**.

Figure S23 shows the differing behavior of complex **5**, regarding electrocatalysis in the presence of AcOH. After the addition of one equivalent, the current of the first reduction, $E_{pc}^1 = -1.51$ V, is increased by 20% only, however, a new peak appears at $E_{pc}^2 = -1.61$ V. Due to the less negative first reduction potential of complex **5** (Figure 3), the two reduction events are separated. Following steps in the catalytic process are similar to complex **3**.

The first reduction of complex **6** in the presence of AcOH exhibits no shift of the potential and remains at $E_{pc}^1 = -1.52$ V (Figure S24), though, the current does not level off until fifteen equivalents. The catalytic process remains around $E_p^{cat2} \approx -2.1$ V, analogous to complexes **2**, **3** and **5**, as well as several examples from the literature.[47]

In order to compare the catalytic performance towards proton reduction of these complexes, the turn-over frequency (TOF) and catalytic efficiency (*C.E.*) were calculated, utilizing equations 1 and 2, respectively.[2,47–49] Table 2 summarizes the obtained data.

$$\frac{I_{cat}}{I_p} = \frac{n}{0.4463}\sqrt{\frac{RT * TOF_{max}}{F\nu}} \quad (1)$$

Table 2. Electrochemical data for the catalysis of complexes **2**, **3**, **5** and **6** ($c = 1$ mmol/L) in the presence of AcOH ($c = 20$ mmol/L). Potentials E are given in V, referenced to the Fc/Fc^+ couple.

complex	E_{cat} [V]	I_{cat}/I_p	k (TOF) [s^{-1}][a]	*C.E.*[b]
2	−2.16	13.18	67	0.66
3	−2.07	11.59	52	0.58
5	−2.11	9.45	35	0.47
6	−2.10	13.15	67	0.66

[a] Calculated by using equation 1 with $\nu = 0.2$ V/s and $n = 2$.[2,48–50]; [b] Calculated by using equation 2.[2]

$$C.E. = \frac{I_{cat}/I_p}{[HA]/[catalyst]} \quad (2)$$

To determine the number of electrons necessary for the hydrogen evolution reaction (HER), plots of the catalytic current (I_{cat}) and peak current (I_p) ratio versus c (AcOH) were illustrated (Figure S25). The observed linear relationship of I_{cat}/I_p to c (AcOH) indicates a second-order dependence of the catalytic pathway.[48] Subsequent use of equation 1 (R – ideal gas constant, T – absolute temperature, F – Faraday's constant, ν – scan rate) leads to TOF values, that are within one magnitude. Complex **2** and **6** exhibit the same TOF value 67 s^{-1} at slightly different reduction potential, although their catalytic processes may vary in their sequence (see Figure 5 and S23). In comparison, the mixed sulfur and selenium complexes show significantly less activity. A similar outcome could be achieved from the *C.E.* calculation, which declares all complexes in the medium scope (0.25–0.75) of efficiency.[47]

Formation and electrochemical behaviour of SAMs on Au and Pt

Previously polished Au and Pt disc electrodes were exposed for 12 h to 1 mM solutions of compounds **2** or **6** in MeCN, and carefully rinsed before electrochemical characterization. CVs of the resulting modified electrodes were performed in an electrolyte solution of 0.1 M [n-Bu_4N][PF_6] in MeCN. On gold (**Au-SAM-2**) a small irreversible signal could be detected with a cathodic current peak potential $E_{pc}^1 = -1.24$ V (Figure S26), a value close to the first reduction wave of compound **2** in solution (in MeCN: $E_{pc}^1 = -1.22$ V vs. SCE). A less well-defined reduction wave at approximately $E_{pc} = -1.25$ V vs. SCE was observed for **Au-SAM-6** (Figure S27). Both results are suggesting the presence of the redox active iron clusters on the electrode surface. However, the lack of reversibility and the shape of the CVs make analysis complicated.

Recently, we have reported the advantage of higher stability of dithiolane SAMs on platinum[51] over gold.[52] In the case of compound **2** the use of a platinum working electrode improved its chemisorption affording **Pt-SAM-2**. Several CVs were performed at a scan speed of $\nu = 10$ V/s (Figure S28) yielding a quasi-reversible wave centered at the formal standard potential $E^{\circ\prime}_1 = -1.52$ V (vs. SCE) (Figure 6A and S29). This signal was attributed to the first reduction $[Fe^{I}Fe^{I}] \rightarrow [Fe^{0}Fe^{I}]$ of the adsorbed clusters, the corresponding E_{pc} being shifted to a more negative value of compared to **Au-SAM-2**.

Analysis of the cathodic peak currents as a function of the scan rate displayed a linear dependence (Figure 6B and S30), characteristic of an electrode-surface confined electroactive species. As in solution no electro-catalytic HER could be observed on this first reduction wave. Unfortunately, the second reduction process could not be probed with a SAM modified electrode. The application of electrode potentials less negative

Research Article
doi.org/10.1002/ejic.202200684

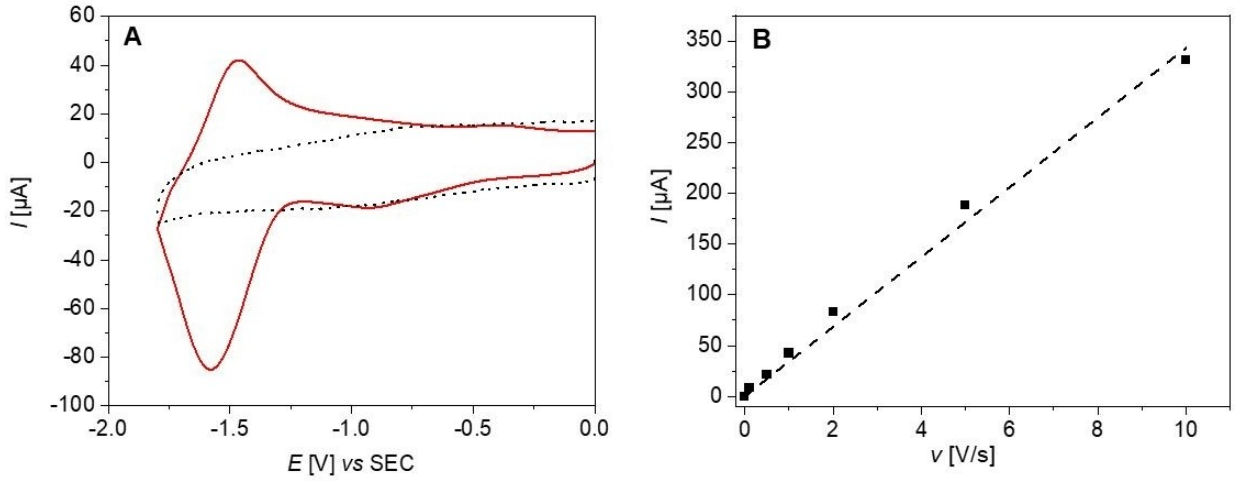

Figure 6. A) Cyclic voltammograms ($\nu = 1$ V/s) of the bare (grey line) and the modified Pt electrode **Pt-SAM-2** (red line) in 0.1 M [n-Bu_4N][PF_6] MeCN solution. WE diameter = 3 mm. B) Plot of the peak current vs. the scan speed of a modified platinum electrode **Pt-SAM-2**.

than $E = -1.8$ V (vs. SCE) afforded the desorption of the SAM via reduction of the thioctic derivatives.

Conclusions

This study focused on the synthesis and electrochemical investigation of lipoic acid ester-based [FeFe] H_2ase model complexes and their formation of SAMs on Au and Pt electrodes. The substantial analysis of the new synthesized complexes **2**, **3**, **5**, and **6** by cyclic voltammetry in the presence and absence of the weak acid AcOH as well as IR SEC experiments revealed a strong influence of lipoic and selenolipoic acid moieties on the electrochemical properties of the [FeFe] H_2ase mimics and their facility to perform catalytic proton reduction under electrocatalytic conditions. Complex **2** exposed a doubled increase in current by adding one equivalent of AcOH, indicating a change of the catalytic cycle in comparison to previously described precursor molecule **1**. A differing behavior was also observed by CV and IR SEC experiments in the absence of acid. However, [FeFe] H_2ase mimics lacked in stability and reversibility.

The substitution of one CO ligand with PPh_3 led to complex **7**, that was further analyzed by X-ray crystallography. The CV exhibited an anticipated shift for the first reduction event by $\Delta E_{pc}{}^1 = 180$ mV, compared to the first reduction event of **2**. The second reduction of both compounds exhibit similar reduction potentials and IR SEC data, that reveal comparable structures and electron densities at the iron cores of both complexes. Further DFT calculation supported investigation might expose the unidentified reduced species.

Furthermore, we were able to form intact SAMs of complexes **2** and **6** on Au and Pt electrodes, that were confirmed by CV experiments. Unfortunately, these SAMs were not able to perform HER in the given potential window terminated by the desorption of the complexes. However, the approach of a catalyst transfer from homogeneous solution to a surface confined system was validated. Stronger covalent bonding of the catalysts to the electrode surface will be necessary for the development of a supported system. Reductive electrografting of diazonium salts onto the electrode may provide catalyst layers being stable within a larger potential range well adapted to the electrocatalytic process.

Experimental Section

The formation of the known complexes **1** and **4** was carried out by other reaction pathways then described in the literature. Therefore, we included the new synthesis routes.

H_2ase mimic 1 – Fe_2S_2

In a Schlenk flask 1,3-disulfanylpropane-2-ol (100 mg, 0.8 mmol) was dissolved in anhydrous toluene (10 mL) and anhydrous NMP (1 mL) under nitrogen atmosphere. After raising the temperature to 50 °C, $Fe_3(CO)_{12}$ (405 mg, 0.8 mmol) was added, and the colour changed from dark green to dark brown within ten minutes while a small amount of gas (CO) was developed. The reaction mixture was cooled down and was put on a column packed with silica and n-hexane. After flushing the column with n-hexane to remove the toluene and NMP, the eluent was changed to cyclo-hexane/THF (6:1). The product was collected from the major red band to give a red, crystalline solid (300 mg, 0.75 mmol, 93 %).[18,21]

^{1}H NMR (400 MHz, $CDCl_3$, 297 K, TMS) δ (ppm) = 3.19–3.07 (m, 1H, C*H*(OH)), 2.81 (dd, $^3J_{H-H} = 13.2$, 4.1 Hz, 2H, CH_aH_b), 1.86 (d, $^3J_{H-H} = 5.6$ Hz, 1H, O*H*), 1.56–1.48 (m, 2H, CH_aH_b); {^{1}H}^{13}C NMR (101 MHz, $CDCl_3$, 297 K, TMS) δ (ppm) = 207.4, 72.9, 29.6.

H_2ase mimic 4 – Fe_2Se_2

In a Schlenk flask 1,3-bis(selenocyanato)propane-2-ol (500 mg, 1.87 mmol) and $Fe_3(CO)_{12}$ (939 mg, 1.87 mmol) were dissolved in THF (60 mL) and the mixture was heated at reflux for 1 h. The solvent was evaporated to dryness under vacuum. The crude

Research Article
doi.org/10.1002/ejic.202200684

product was purified by column chromatography (cyclo-hexane/THF 4:1) to get a red oil from the major red fraction. Recrystallization from DCM/*n*-pentane at 0 °C gave complex **4** as red crystalline product (402 mg, 0.81 mmol, 43 %).[19,23]

^{1}H NMR (600 MHz, CD_2Cl_2, 297 K, TMS) δ (ppm) = 3.02–2.94 (m, 1H, C*H*(OH)), 2.85 (br dd, $^3J_{H-H}$ = 11.6, 2.8 Hz, 2H, CH_aH$_b$), 2.05 (br d, $^3J_{H-H}$ = 5.5 Hz, 1H, O*H*), 1.55 (br t, $^3J_{H-H}$ = 11.3 Hz, 2H, CH$_a$$H_b$); {^{1}H}^{13}C NMR (151 MHz, CD_2Cl_2, 297 K, TMS) δ (ppm) = 209.4, 72.9, 19.7; {^{1}H}^{77}Se (76 MHz, CD_2Cl_2, 297 K) δ (ppm) = 202.04; elemental analysis calcd. (%) for $C_9H_6Fe_2O_7Se_2$: C 21.80, H 1.22; found: C 22.09, H 1.12.

General procedure: Steglich esterification

In a Schlenk flask complex **1** or **4** (0.2 mmol), 1,2-Dithiolane-3-pentanoic acid or 1,2-diselenolane-3-pentanoic acid (0.22 mmol, 1.1 eq) and DMAP (27 mg, 0.2 mmol) were stirred in 10 mL anhydrous DCM for 5 minutes. DCC (46 mg, 0.22 mmol) was dissolved in 2 mL anhydrous DCM and was added in one portion. The resulting mixture was stirred overnight. The desired complexes **2**, **3**, **5** and **6** could be isolated as red high-viscous oils after purification via column chromatography (*n*-hexane/DCM 1:1).[20]

H_2ase mimic 2 – Fe_2S_2~S_2

Yield 102 mg, 87 %; ^{1}H NMR (400 MHz, $CDCl_3$, 297 K) δ (ppm) = 4.37–4.22 (m, 1H, C*H*(O)), 3.55 (quin, $^3J_{H-H}$ = 6.8 Hz, 1H, C*H*(S)), 3.22–3.08 (m, 2H, CH_2(S)), 2.75 (dd, $^3J_{H-H}$ = 12.9, $^3J_{H-H}$ = 4.1 Hz, 2H, CH_aH$_b$-(CHO)), 2.46 (dq, $^3J_{H-H}$ = 12.5, $^3J_{H-H}$ = 6.3 Hz, 1H, CH_aH$_b$(CH$_2$S)), 2.25 (t, $^3J_{H-H}$ = 7.3 Hz, 2H, CH_2(C=O)), 1.90 (dq, $^3J_{H-H}$ = 13.0, $^3J_{H-H}$ = 6.8 Hz, 1H, CH$_a$$H_b$(CH$_2$S)), 1.71–1.53 (m, 6H, COCH$_2$CH_2CH$_2$CH_2 + CH$_a$$H_b$(CHO), 1.51–1.37 (m, 2H, CO(CH$_2$)$_2$CH_2); {^{1}H}^{13}C NMR (101 MHz, $CDCl_3$, 297 K) δ (ppm) = 207.2, 171.6, 73.4, 56.3, 40.2, 38.5, 34.5, 33.8, 28.6, 26.9, 24.5; MS (ESI positive mode): m/z = 612.8 (M + Na$^+$, calcd. 612.8); IR (ATR, $CHCl_3$, 297 K) $\tilde{\nu}$ (cm^{-1}) = 2077, 2036, 1993; elemental analysis calcd. (%) for $C_{17}H_{18}Fe_2O_8S_4$: C 34.59, H 3.07, S 21.73; found: C 34.70, H 2.99, S 21.80.

H_2ase mimic 3 – Fe_2S_2~Se_2

Yield 122 mg, 90 %; ^{1}H NMR (400 MHz, $CDCl_3$, 297 K) δ (ppm) = 4.31 (tt, $^3J_{H-H}$ = 11.1, 4.3 Hz, 1H, C*H*(O)), 3.90 (ddt, $^3J_{H-H}$ = 9.3, 7.5, 4.9 Hz, 1H, C*H*(Se)), 3.38–3.29 (m, 2H, CH_2Se), 3.02–2.90 (m, 1H; CH_aH$_b$-(CH$_2$Se)), 2.77 (dd, $^3J_{H-H}$ = 12.9, 4.4 Hz, 2H, CH_aH$_b$(CHO)), 2.58–2.47 (m, 1H, CH$_a$$H_b$(CH$_2$Se)), 2.27 (t, $^3J_{H-H}$ = 7.5 Hz, 2H, CH_2(C=O)), 1.85–1.56 (m, 6H, COCH$_2$CH_2CH$_2$CH_2 + CH$_a$$H_b$(CHO)), 1.49–1.38 (m, 2H, CO(CH$_2$)$_2$CH_2); {^{1}H}^{13}C NMR (101 MHz, $CDCl_3$, 297 K) δ (ppm) = 207.1, 171.6, 73.4, 52.5, 45.7, 35.3, 33.8, 29.6, 29.4, 26.9, 24.4; {^{1}H}^{77}Se (76 MHz, $CDCl_3$, 297 K) δ (ppm) = 376.09, 299.67; MS (EI): m/z = 600 (M-3CO), 572 (M-4CO), 544 (M-5CO), 516 (M-6CO); IR (ATR, $CHCl_3$, 297 K) $\tilde{\nu}$ (cm^{-1}) = 2077, 2037, 1995; elemental analysis calcd. (%) for $C_{17}H_{18}Fe_2O_8S_2Se_2$ 0.08 C_6H_{14}: C 30.41, H 2.79, S 9.28; found: C 30.38, H 2.71, S 8.97.

H_2ase mimic 5 – Fe_2Se_2~S_2

Yield 92 mg, 67 %; ^{1}H NMR (400 MHz, $CDCl_3$, 297 K) δ (ppm) = 4.16 (br t, $^3J_{H-H}$ = 11.0 Hz, 1H, C*H*(O)), 3.61–3.50 (m, 1H, C*H*(S)), 3.22–3.08 (m, 2H, CH_2(S)), 2.80 (br d, $^3J_{H-H}$ = 10.6 Hz, 2H, CH_aH$_b$(CHO)), 2.46 (br dd, $^3J_{H-H}$ = 12.3, 6.2 Hz, 1H, CH_aH$_b$(CH$_2$S)), 2.25 (t, $^3J_{H-H}$ = 6.6 Hz, 2H, CH_2(C=O)), 1.90 (br dd, $^3J_{H-H}$ = 12.3, 7.0 Hz, 2H, CH$_a$$H_b$(CH$_2$S)), 1.72–1.56 (m, 6H, COCH$_2$CH_2CH$_2$CH_2 + CH$_a$$H_b$(CHO)), 1.49–1.38 (m, 2H, CO(CH$_2$)$_2$CH_2); {^{1}H}^{13}C NMR (151 MHz, $CDCl_3$, 297 K) δ (ppm) = 208.3, 171.5, 73.7, 56.3, 40.2, 38.5, 34.5, 33.8, 28.6, 24.4, 16.3; {^{1}H}^{77}Se (76 MHz, $CDCl_3$, 297 K) δ (ppm) = 205.4; MS (EI): m/z = 600 (M-3CO), 516 (M-6CO); IR (ATR, $CHCl_3$, 297 K) $\tilde{\nu}$ (cm^{-1}) = 2070, 2031, 1992; elemental analysis calcd. (%) for $C_{17}H_{18}Fe_2O_8S_2Se_2$ 0.125 C_6H_{14}: C 30.68, H 2.87, S 9.28; found: C 30.66, H 2.77, S 8.98.

H_2ase mimic 6 – Fe_2Se_2~Se_2

Yield 82 mg, 52 %; ^{1}H NMR (400 MHz, $CDCl_3$, 297 K) δ (ppm) = 4.16 (tt, $^3J_{H-H}$ = 11.5, 3.5 Hz, 1H, C*H*(O)), 3.89 (ddt, $^3J_{H-H}$ = 9.2, 7.6, 4.8 Hz, 1H, C*H*(Se)), 3.39–3.25 (m, 2H, CH_2Se), 2.95 (dq, $^3J_{H-H}$ = 13.6, 5.4 Hz 1H; CH_aH$_b$(CH$_2$Se)), 2.87–2.72 (m, 2H, CH_aH$_b$(CHO)), 2.57–2.46 (m, 1H, CH$_a$$H_b$(CH$_2$Se)), 2.25 (t, $^3J_{H-H}$ = 7.5 Hz, 2H, CH_2(C=O)), 1.85–1.55 (m, 6H, COCH$_2$CH_2CH$_2$CH_2 + CH$_a$$H_b$(CHO)), 1.49–1.36 (m, 2H, CO-(CH$_2$)$_2$CH_2); {^{1}H}^{13}C NMR (101 MHz, $CDCl_3$, 297 K) δ (ppm) = 208.3, 208.3, 171.5, 73.7, 52.5, 45.7, 35.2, 33.8, 29.6, 29.3, 24.4, 16.3; {^{1}H}^{77}Se (76 MHz, $CDCl_3$, 297 K) δ (ppm) = 376.27, 299.80, 205.46; MS (EI): m/z = 750 (M–CO),696 (M-3CO), 640 (M-5CO), 612 (M-6CO); IR (ATR, $CHCl_3$, 297 K) $\tilde{\nu}$ (cm^{-1}) = 2069, 2029, 1989; elemental analysis calcd. (%) for $C_{17}H_{18}Fe_2O_8Se_4$: C 26.25, H 2.33; found: C 26.69, H 2.76.

H_2ase mimic 7 – $Fe_2S_2PPh_3$~S_2

In a Schlenk flask **2** (100 mg, 0.17 mmol) and trimethylamine *N*-oxide dihydrate (19 mg, 0.17 mmol) were stirred in 10 mL anhydrous MeCN for 10 minutes. PPh_3 (44 mg, 0.17 mmol) was added to the brown solution and the reaction mixture was stirred for another hour. The solvent was removed under reduced pressure and the crude product was purified by column chromatography (*n*-hexane/THF 2:1) to get **7** as a brown, oxygen sensitive solid (77 mg, 0.09 mmol, 55 %).[25]

^{1}H NMR (400 MHz, CD_2Cl_2, 297 K) δ (ppm) = 7.73–7.59 (m, 6H, Ar–*H*), 7.51–7.39 (m, 9H, Ar–*H*), 3.59–3.44 (m, 2H, C*H*(O) + C*H*(S)), 3.21–3.06 (m, 2H, CH_2(S)), 2.43 (m, 1H, CH_aH$_b$(CH$_2$S)), 2.21 (m, 2H, CH_aH$_b$(CHO), 2.01 (t, $^3J_{H-H}$ = 7.3 Hz, 2H, CH_2(C=O)), 1.88 (m, 1H, CH$_a$$H_b$(CH$_2$S)), 1.73–1.50 (m, 4H, COCH$_2$CH_2CH$_2$CH_2), 1.48–1.37 (m, 4H, CH$_a$$H_b$(CHO) - + CO(CH$_2$)$_2CH_2$); {^{1}H}^{13}C NMR (101 MHz, CD_2Cl_2, 297 K) δ (ppm) = 214.6, 171.4, 136.1, 135.8, 134.0, 130.9, 129.0, 74.4, 56.9, 40.8, 39.1, 35.0, 34.3, 29.1, 27.3, 25.1; {^{1}H}^{31}P NMR (162 MHz, CD_2Cl_2, 297 K) δ (ppm) = 63.17; MS (ESI positive mode): m/z = 846.7 (M + Na$^+$, calcd. 846.9); IR (ATR, $CHCl_3$, 297 K) $\tilde{\nu}$ (cm^{-1}) = 2045, 1982, 1961, 1937; elemental analysis calcd. (%) for $C_{34}H_{33}Fe_2O_7PS_4$ 0.125 C_6H_{14}: C 49.97, H 4.19, S 15.35; found: C 50.22, H 4.21, S 15.40.

Deposition Numbers 2209004 (for selenolipoic acid) and 2209005 (for 7) contain the supplementary crystallographic data for this paper. These data are provided free of charge by the joint Cambridge Crystallographic Data Centre and Fachinformationszentrum Karlsruhe Access Structures service www.ccdc.cam.ac.uk/structures.

Acknowledgements

Financial support by the German Science Foundation (DFG) via the TRR234 CataLight is gratefully acknowledged (project number 364549901, project A2), as well as the support from the French GDR 2088 BIOMIM . We are thankful to Dr. Kupfer and Dr. Abul-Futouh for important discussions. Open Access funding enabled and organized by Projekt DEAL.

Conflict of Interest

The authors declare no conflict of interest.

Data Availability Statement

The data that support the findings of this study are available from the corresponding author upon reasonable request.

Keywords: cyclic voltammetry · electrode modification · [FeFe] hydrogenase mimics · monolayers · spectroelectrochemistry

[1] a) W. Weigand, *Phosphorus Sulfur Silicon Relat. Elem.* **2019**, *194*, 63 b) H.-L. Wu, X.-B. Li, C.-H. Tung, L.-Z. Wu, *Chem. Commun.* **2020**, *56*, 1549; c) L. Sun, C. Duboc, K. Shen, *ACS Catal.* **2022**, *12*, 9159; d) J. T. Kleinhaus, F. Wittkamp, S. Yadav, D. Siegmund, U.-P. Apfel, *Chem. Soc. Rev.* **2021**, *50*, 1668; e) Y. Li, T. B. Rauchfuss, *Chem. Rev.* **2016**, *116*, 704; f) S. Gao, W. Fan, Y. Liu, D. Jiang, Q. Duan, *Int. J. Hydrogen Energy* **2020**, *45*, 430; g) W. Lubitz, H. Ogata, O. Rüdiger, E. Reijerse, *Chem. Rev.* **2014**, *114*, 408; h) J. Noth, J. Esselborn, J. Güldenhaupt, A. Brünje, A. Sawyer, U.-P. Apfel, K. Gerwert, E. Hofmann, M. Winkler, T. Happe, *Angew. Chem. Int. Ed.* **2016**, *55*, 839; i) J.-F. Capon, F. Gloaguen, F. Y. Pétillon, P. Schollhammer, J. Talarmin, *Coord. Chem. Rev.* **2009**, *253*, 147; j) Y.-C. Liu, T.-H. Yen, K.-T. Chu, M.-H. Chiang, *Comments Inorg. Chem.* **2016**, *36*, 14; k) F. Wang, W.-G. Wang, H.-Y. Wang, G. Si, C.-H. Tung, L.-Z. Wu, *ACS Catal.* **2012**, *2*, 40; l) A. Zamader, B. Reuillard, J. Pécaut, L. Billon, A. Bousquet, G. Berggren, V. Artero, *Chem. Eur. J.* **2022**, *28*, e20220226.

[2] S. Gao, Y. Liu, Y. Shao, D. Jiang, Q. Duan, *Coord. Chem. Rev.* **2020**, *402*, 213081.

[3] M. B. Wilker, J. K. Utterback, S. Greene, K. A. Brown, D. W. Mulder, P. W. King, G. Dukovic, *J. Phys. Chem. C* **2018**, *122*, 741.

[4] J. C. Ruth, A. M. Spormann, *ACS Catal.* **2021**, *11*, 5951.

[5] R. E. Treviño, J. W. Slater, H. S. Shafaat, *ACS Appl. Energ. Mater.* **2020**, *3*, 11099.

[6] a) J. C. Ruth, R. D. Milton, W. Gu, A. M. Spormann, *Chem. Eur. J.* **2020**, *26*, 7323; b) T. Yu, Y. Zeng, J. Chen, X. Zhang, G. Yang, Y. Li, *J. Mater. Chem. A* **2014**, *2*, 20500; c) S. K. Ibrahim, X. Liu, C. Tard, C. J. Pickett, *Chem. Commun.* **2007**, 1535; d) M. Karayilan, W. P. Brezinski, K. E. Clary, D. L. Lichtenberger, R. S. Glass, J. Pyun, *Angew. Chem. Int. Ed.* **2019**, *58*, 7537; e) D. Heine, C. Pietsch, U. S. Schubert, W. Weigand, *J. Polym. Sci. Part A* **2013**, *51*, 2171; f) L. Wang, Z. Xiao, X. Ru, X. Liu, *RSC Adv.* **2011**, *1*, 1211; g) E. Xu, Z. Xiao, H. Liu, L. Long, L. Li, X. Liu, *RSC Adv.* **2012**, *2*, 10171; h) D. Zhu, Z. Xiao, X. Liu, *Int. J. Hydrogen Energy* **2015**, *40*, 5081; i) X. Zhu, W. Zhong, X. Liu, *Int. J. Hydrogen Energy* **2016**, *41*, 14068.

[7] K. Sakai, H. Xia, Y. Kitazumi, O. Shirai, K. Kano, *Electrochim. Acta* **2018**, *271*, 305.

[8] V. Vijaikanth, J.-F. Capon, F. Gloaguen, P. Schollhammer, J. Talarmin, *Electrochem. Commun.* **2005**, *7*, 427.

[9] a) M. E. Ahmed, S. Dey, B. Mondal, A. Dey, *Chem. Commun.* **2017**, *53*, 8188; b) A. Le Goff, V. Artero, R. Metayé, F. Moggia, B. Jousselme, M. Razavet, P. D. Tran, S. Palacin, M. Fontecave, *Int. J. Hydrogen Energy* **2010**, *35*, 10790.

[10] R. Zaffaroni, R. J. Detz, J. I. van der Vlugt, J. N. H. Reek, *ChemSusChem* **2018**, *11*, 209.

[11] M. Wen, H.-L. Wu, J.-X. Jian, X.-Z. Wang, X.-B. Li, B. Chen, C.-H. Tung, L.-Z. Wu, *ChemPhotoChem* **2017**, *1*, 260.

[12] a) J. Sanabria-Chinchilla, A. Javier, D. Crouthers, J. H. Baricuatro, M. Y. Darensbourg, M. P. Soriaga, *Electrocatalysis* **2014**, *5*, 5; b) O. Rüdiger, C. Gutiérrez-Sánchez, D. Olea, I. A. C. Pereira, M. Vélez, V. M. Fernández, A. L. De Lacey, *Electroanalysis* **2010**, *22*, 776; c) X. Ru, X. Zeng, Z. Li, D. J. Evans, C. Zhan, Y. Tang, L. Wang, X. Liu, *J. Polym. Sci. Part A* **2010**, *48*, 2410; d) D. Millo, M.-E. Pandelia, T. Utesch, N. Wisitruangsakul, M. A. Mroginski, W. Lubitz, P. Hildebrandt, I. Zebger, *J. Phys. Chem. B* **2009**, *113*, 15344; e) C. Madden, M. D. Vaughn, I. Díez-Pérez, K. A. Brown, P. W. King, D. Gust, A. L. Moore, T. A. Moore, *J. Am. Chem. Soc.* **2012**, *134*, 1577; f) C. Gutiérrez-Sánchez, D. Olea, M. Marques, V. M. Fernández, I. A. C. Pereira, M. Vélez, A. L. De Lacey, *Langmuir* **2011**, *27*, 6449; g) B. Chmielowiec, F. H. Saadi, J. H. Baricuatro, A. Javier, Y.-G. Kim, G. Sun, M. Y. Darensbourg, M. P. Soriaga, *J. Electroanal. Chem.* **2014**, *716*, 63; h) A. Nayek, M. E. Ahmed, S. Samanta, S. Dinda, S. Patra, S. G. Dey, A. Dey, *J. Am. Chem. Soc.* **2022**, *144*, 8402; i) X. Zhang, L. Liu, W. Cao, D. Lv, *Catal. Lett.* **2020**, *150*, 3409; j) M. E. Ahmed, D. Saha, L. Wang, M. Gennari, S. Ghosh Dey, V. Artero, A. Dey, C. Duboc, *ChemElectroChem* **2021**, *8*, 1674; k) M. Watanabe, Y. Honda, H. Hagiwara, T. Ishihara, *J. Photochem. Photobiol. C* **2017**, *33*, 1; l) M. Cao, Z. Wang, J. Zhang, S. Xu, S. Zhang, X. Dai, X. Jiang, *Inorg. Chim. Acta* **2018**, *469*, 402.

[13] a) P. D. Tran, V. Artero, M. Fontecave, *Energy Environ. Sci.* **2010**, *3*, 727; b) L. J. Antila, P. Ghamgosar, S. Maji, H. Tian, S. Ott, L. Hammarström, *ACS Energy Lett.* **2016**, *1*, 1106; c) C. M. Thomas, O. Rüdiger, T. Liu, C. E. Carson, M. B. Hall, M. Y. Darensbourg, *Organometallics* **2007**, *26*, 3976.

[14] R. Sahli, C. Fave, N. Raouafi, K. Boujlel, B. Schöllhorn, B. Limoges, *Langmuir* **2013**, *29*, 5360.

[15] a) K. M. Joly, G. Mirri, Y. Willener, S. L. Horswell, C. J. Moody, J. H. R. Tucker, *J. Org. Chem.* **2010**, *75*, 2395; b) A. G. Young, D. P. Green, A. J. McQuillan, *Langmuir* **2007**, *23*, 12923.

[16] a) J. Hildebrandt, R. Trautwein, D. Kritsch, N. Häfner, H. Görls, M. Dürst, I. B. Runnebaum, W. Weigand, *Dalton Trans.* **2019**, *48*, 936; b) X. Liu, M.-C. Barth, K. Cseh, C. R. Kowol, M. A. Jakupec, B. K. Keppler, D. Gibson, W. Weigand, *Chem. Biodiversity* **2022**, *19*, e202200695.

[17] a) C. V. Krishnan, M. Garnett, *Int. J. Electrochem. Sci.* **2011**, *6*, 3607; b) B. Ke, *Biochim. Biophys. Acta* **1957**, *25*, 650.

[18] U.-P. Apfel, Y. Halpin, H. Görls, J. G. Vos, B. Schweizer, G. Linti, W. Weigand, *Chem. Biodiversity* **2007**, *4*, 2138.

[19] L.-C. Song, W. Gao, C.-P. Feng, D.-F. Wang, Q.-M. Hu, *Organometallics* **2009**, *28*, 6121.

[20] B. Neises, W. Steglich, *Angew. Chem. Int. Ed.* **1978**, *17*, 522.

[21] S. Benndorf, E. Hofmeister, M. Wächtler, H. Görls, P. Liebing, K. Peneva, S. Gräfe, S. Kupfer, B. Dietzek-Ivanšić, W. Weigand, *Eur. J. Inorg. Chem.* **2022**, *3*, e202100959.

[22] I. Cordova-Reyes, H. Hu, J.-H. Gu, E. Vandenhoven, A. Mohammed, S. Holdcroft, B. M. Pinto, *Can. J. Chem.* **1996**, *74*, 533.

[23] M. K. Harb, U.-P. Apfel, J. Kübel, H. Görls, G. A. N. Felton, T. Sakamoto, D. H. Evans, R. S. Glass, D. L. Lichtenberger, M. El-khateeb, W. Weigand, *Organometallics* **2009**, *28*, 6666.

[24] M. K. Harb, H. Alshurafa, M. El-khateeb, A. Al-Zuheiri, H. Görls, H. Abul-Futouh, W. Weigand, *ChemistrySelect* **2018**, *3*, 8867.

[25] H. Abul-Futouh, L. R. Almazahreh, S. J. Abaalkhail, H. Görls, S. T. Stripp, W. Weigand, *New J. Chem.* **2021**, *45*, 36.

[26] L.-C. Song, X.-F. Liu, J.-B. Ming, J.-H. Ge, Z.-J. Xie, Q.-M. Hu, *Organometallics* **2010**, *29*, 610.

[27] H. Abul-Futouh, M. El-khateeb, H. Görls, K. J. Asali, W. Weigand, *Dalton Trans.* **2017**, *46*, 2937.

[28] U.-P. Apfel, Y. Halpin, H. Görls, J. G. Vos, B. Schweizer, G. Linti, W. Weigand, *Chem. Biodiversity* **2007**, *4*, 2138.

[29] a) U.-P. Apfel, Y. Halpin, M. Gottschaldt, H. Görls, J. G. Vos, W. Weigand, *Eur. J. Inorg. Chem.* **2008**, *2008*, 5112; b) L.-C. Song, B. Gai, H.-T. Wang, Q.-M. Hu, *J. Inorg. Biochem.* **2009**, *103*, 805; c) R. Trautwein, L. R. Almazahreh, H. Görls, W. Weigand, *Z. Anorg. Allg. Chem.* **2013**, *639*, 1512; d) C. Figliola, L. Male, P. N. Horton, M. B. Pitak, S. J. Coles, S. L. Horswell, R. S. Grainger, *Organometallics* **2014**, *33*, 4449.

[30] R. Trautwein, L. R. Almazahreh, H. Görls, W. Weigand, *Dalton Trans.* **2015**, *44*, 18780.

[31] a) H. Abul-Futouh, S. J. Abaalkhail, M. K. Harb, H. Görls, W. Weigand, *Polyhedron* **2021**, *207*, 115382; b) F. Wang, M. Wang, X. Liu, K. Jin, W. Dong, L. Sun, *Dalton Trans.* **2007**, *34*, 3812; c) L.-C. Song, J.-H. Ge, X.-G. Zhang, Y. Liu, Q.-M. Hu, *Eur. J. Inorg. Chem.* **2006**, *2006*, 3204; d) G. Durgaprasad, R. Bolligarla, S. K. Das, *J. Organomet. Chem.* **2011**, *696*, 3097; e) C.-G. Li, Y. Zhu, X.-X. Jiao, X.-Q. Fu, *Polyhedron* **2014**, *67*, 416; f) P. Li, M. Wang, C. He, G. Li, X. Liu, C. Chen, B. Åkermark, L. Sun, *Eur. J. Inorg. Chem.* **2005**, 2506; g) M. L. Singleton, R. M. Jenkins, C. L. Klemashevich, M. Y. Darensbourg, *C. R. Chim.* **2008**, *11*, 861; h) W.-G. Wang, H.-Y. Wang, G. Si, C.-H. Tung, L.-Z. Wu, *Dalton Trans.* **2009**, 2712; i) Z. Wang, W. Jiang, J. Liu, W. Jiang, Y. Wang, B. Åkermark, L. Sun, *J. Organomet. Chem.* **2008**, *693*, 2828.

[32] T. Liu, B. Li, M. L. Singleton, M. B. Hall, M. Y. Darensbourg, *J. Am. Chem. Soc.* **2009**, *131*, 8296.

[33] S. J. Borg, T. Behing, S. P. Best, M. Razavet, X. Liu, C. J. Pickett, *J. Am. Chem. Soc.* **2004**, *126*, 16988.

[34] K. Nakamoto, in *Infrared and Raman Spectra of Inorganic and Coordination Compounds, Part B: Applications in Coordination, Organometallic, and Bioinorganic Chemistry*, John Wiley & Sons, New York, **1997**.

[35] S. P. Best, *Coord. Chem. Rev.* **2005**, *249*, 1536.

[36] M. Krejčik, M. Daněk, F. Hartl, *J. Electroanal. Chem.* **1991**, *317*, 179.
[37] J. P. H. Oudsen, B. Venderbosch, D. J. Martin, T. J. Korstanje, J. N. H. Reek, M. Tromp, *Phys. Chem. Chem. Phys.* **2019**, *21*, 14638.
[38] S. J. Borg, J. W. Tye, M. B. Hall, S. P. Best, *Inorg. Chem.* **2007**, *46*, 384.
[39] a) S. Wang, A. Aster, M. Mirmohades, R. Lomoth, L. Hammarström, *Inorg. Chem.* **2018**, *57*, 768; b) E. C. F. Schippers, S. S. Nurttila, J.-P. H. Oudsen, M. Tromp, W. I. Dzik, J. I. van der Vlugt, J. N. H. Reek, *Eur. J. Inorg. Chem.* **2019**, *2019*, 2510; c) D. Chong, I. P. Georgakaki, R. Mejia-Rodriguez, J. Sanabria-Chinchilla, M. P. Soriaga, M. Y. Darensbourg, *Dalton Trans.* **2003**, *21*, 4158.
[40] M. Mirmohades, S. Pullen, M. Stein, S. Maji, S. Ott, L. Hammarström, R. Lomoth, *J. Am. Chem. Soc.* **2014**, *136*, 17366.
[41] P. S. Singh, H. C. Rudbeck, P. Huang, S. Ezzaher, L. Eriksson, M. Stein, S. Ott, R. Lomoth, *Inorg. Chem.* **2009**, *48*, 10883.
[42] S. J. Borg, S. K. Ibrahim, C. J. Pickett, S. P. Best, *C. R. Chim.* **2008**, *11*, 852.
[43] D. J. Curran, P. B. Graham, M. D. Rausch, *Organometallics* **1993**, *12*, 2380.
[44] G. A. N. Felton, A. K. Vannucci, J. Chen, L. T. Lockett, N. Okumura, B. J. Petro, U. I. Zakai, D. H. Evans, R. S. Glass, D. L. Lichtenberger, *J. Am. Chem. Soc.* **2007**, *129*, 12521.
[45] a) J.-F. Capon, S. Ezzaher, F. Gloaguen, F. Y. Pétillon, P. Schollhammer, J. Talarmin, T. J. Davin, J. E. McGrady, K. W. Muir, *New J. Chem.* **2007**, *31*, 2052; b) S. Roy, T.-A. D. Nguyen, L. Gan, A. K. Jones, *Dalton Trans.* **2015**, *44*, 14865.
[46] a) C. Greco, G. Zampella, L. Bertini, M. Bruschi, P. Fantucci, L. de Gioia, *Inorg. Chem.* **2007**, *46*, 108; b) J. Chen, A. K. Vannucci, C. A. Mebi, N. Okumura, S. C. Borowski, M. Swenson, L. T. Lockett, D. H. Evans, R. S. Glass, D. L. Lichtenberger, *Organometallics* **2010**, *29*, 5330; c) L. Schwartz, P. S. Singh, L. Eriksson, R. Lomoth, S. Ott, *C. R. Chim.* **2008**, *11*, 875; d) J.-F. Capon, F. Gloaguen, P. Schollhammer, J. Talarmin, *J. Electroanal. Chem.* **2006**, *595*, 47.
[47] G. A. Felton, C. A. Mebi, B. J. Petro, A. K. Vannucci, D. H. Evans, R. S. Glass, D. L. Lichtenberger, *J. Organomet. Chem.* **2009**, *694*, 2681.
[48] P.-H. Zhao, M.-Y. Hu, J.-R. Li, Z.-Y. Ma, Y.-Z. Wang, J. He, Y.-L. Li, X.-F. Liu, *Organometallics* **2019**, *38*, 385.
[49] D. H. Pool, D. L. DuBois, *J. Organomet. Chem.* **2009**, *694*, 2858.
[50] M. E. Ahmed, A. Dey, *Curr. Opin. Electrochem.* **2019**, *15*, 155.
[51] H. Hijazi, E. Levillain, B. Schöllhorn, C. Fave, *ChemElectroChem* **2022**, *9*, e20220019.
[52] H. Hijazi, A. Vacher, S. Groni, D. Lorcy, E. Levillain, C. Fave, B. Schöllhorn, *Chem. Commun.* **2019**, *55*, 1983.

Manuscript received: November 4, 2022
Revised manuscript received: December 30, 2022
Accepted manuscript online: January 10, 2023